

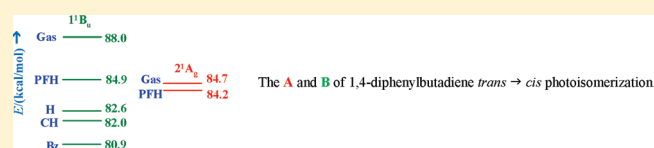
Medium Effects on the Direct Cis–Trans Photoisomerization of 1,4-Diphenyl-1,3-butadiene in Solution

Jack Saltiel,^{*,†} Talapragada R. S. Krishna,[†] Kritapas Laohhasurayotin,[†] Yanjun Ren,[†] Kathleen Phipps,[†] Paul H. Davis,[‡] and W. Atom Yee[‡]

[†]Departments of Chemistry and Biochemistry, Florida State University, Tallahassee, Florida 32306-4390, United States

[‡]Santa Clara University, Santa Clara, California 95053-0365, United States

ABSTRACT: Quantum yields for the photoisomerization of *trans,trans*-1,4-diphenyl-1,3-butadiene (*tt*-DPB), determined in benzene, cyclohexane, methylcyclohexane, hexane, and perfluorohexane, confirm the low values reported earlier for benzene and cyclohexane and reveal even lower values in the last two solvents. In contrast to *trans*-stilbene (*t*-St), fluorescence and torsional relaxation leading to photoisomerization do not account exclusively for S_1 *tt*-DPB decay. Competing radiationless singlet excited-state decay pathways exist in *tt*-DPB, which do not lead to photoisomerization and may not involve large-amplitude torsional motions. Our results invalidate analyses of *tt*-DPB fluorescence quantum yields and lifetimes that assign all radiationless decay to the isomerization channel. Gas-phase chromatography analysis of *tt*-DPB photoisomerization in hexane shows the reaction to be concentration-independent and reveals, for the first time, a significant, two-bond photoisomerization pathway, $\phi_{tt \rightarrow tc} = 0.092$ and $\phi_{tt \rightarrow cc} = 0.020$. The dominant one-bond-twist (OBT) process is accompanied by a bicycle pedal (BP) process that accounts for almost 20% of *tt*-DPB photoisomerization. The OBT *tt*-DPB photoisomerization quantum yield is largest in benzene (Bz) and smallest in perfluorohexane (PFH). Contrary to expectations, reduction in medium friction in PFH is accompanied by a decrease in $\phi_{tt \rightarrow tc}$. The $1^1B_u/2^1A_g$ order and energy gap appear to control the contribution of torsional relaxation to radiationless decay. Lowering the 1^1B_u energy as in Bz favors photoisomerization. Reversal of the $1^1B_u/2^1A_g$ order in PFH is accompanied by short τ_f and small ϕ_f and $\phi_{tt \rightarrow tc}$ values that suggest the presence of competing $2^1A_g \rightarrow 1^1A_g$ relaxation paths that are unproductive with respect to photoisomerization. We conclude that the Birks extension to diphenylpolyenes of the Orlandi–Siebrand cis–trans photoisomerization mechanism is not valid. Photoisomerization appears to occur in the 1^1B_u state, and we argue that this applies to *t*-St as well.



INTRODUCTION

The photochemistry and photophysics of α,ω -diphenylpolyenes have been studied extensively because these molecules are considered to be models for the retinyl polyenes that are related to vitamin A and the visual pigments.^{1,2} A small intrinsic torsional energy barrier in the lowest excited singlet state (S_1) of *t*-St was proposed by one of us long ago.³ It accounts for the temperature dependencies of photoisomerization quantum yields⁴ and fluorescence quantum yields⁵ and lifetimes.^{6,7} On the basis of symmetry, excited states of planar all-*trans*-diphenylpolyenes are designated as n^1A_g or n^1B_u . Hudson and Kohler first pointed out that, in contrast to *t*-St, for which the lowest excited state that is observed in both absorption and fluorescence is the 1^1B_u state, S_1 for longer α,ω -diphenylpolyenes is the 2^1A_g state.^{8,9} Thus, for the all-*trans* isomers of 1,6-diphenyl-1,3,5-hexatriene (*ttt*-DPH) and 1,8-diphenyl-1,3,5,7-octatetraene, excitation to the 1^1B_u state gives rise to the vibronically resolved bands of the lowest-energy-allowed electronic transition in the absorption spectrum, but fluorescence comes predominantly from the energetically lower-lying 2^1A_g state.^{8,9}

Orlandi and Siebrand (OS) attributed the torsional energy barrier along the isomerization coordinate of *t*-St to an assumed crossing of S_1 and S_2 potential energy curves whose symmetries

are 1^1B_u and 2^1A_g , respectively.¹⁰ The energies of the 1^1B_u and 2^1A_g states were proposed to increase and decrease, respectively, with twisting about the central bond. The OS photoisomerization model was extended to the higher members of the diphenylpolyene family by Birks,¹¹ who interpreted the temperature dependencies of their fluorescence quantum yields and lifetimes by assuming that fluorescence and photoisomerization are the sole significant decay processes, as in *t*-St.⁹

Because a large-amplitude motion is associated with their photoisomerization, *t*-St and *trans,trans*-1,4-diphenyl-1,3-butadiene (*tt*-DPB), the two lowest members of the series, have been widely used as probes for testing theories on medium effects. In the main, those studies have followed Birks' lead in assigning radiationless decay rate constants inferred from fluorescence quantum yields and lifetimes to torsional relaxation, exclusively.^{12–16}

We have shown that the assumption of photoisomerization/fluorescence complementarity is not valid for the 1,6-diphenyl-1,3,5-hexatriene isomers.¹⁷ The results presented in this paper on the photoisomerization of the DPB isomers show that the

Received: December 2, 2010

Revised: January 21, 2011

Published: February 25, 2011

photoisomerization/fluorescence complementarity assumption fails in this case also.

EXPERIMENTAL SECTION

Materials. *tt*-DPB (Aldrich, reagent) was purified by chromatography on alumina and recrystallized from ethanol; for experiments at Santa Clara University (SCU), it was recrystallized twice from ethanol. *cc*-DPB was synthesized using a modification of a known procedure,¹⁸ as previously described.¹⁹ *ct*-DPB was prepared photochemically from *tt*-DPB followed by chromatographic separation of the photostationary mixture by a procedure analogous to that previously described.²⁰ Cyclohexane (Fisher, HPLC grade) was distilled over P₂O₅ before use. Methylcyclohexane (Aldrich, spectrograde) was used as received. Perfluorohexane (Aldrich) was refluxed over KMnO₄ and distilled. The sources of other materials and the purification methods used in this work were as previously described.^{20–22}

Irradiation Procedures. Sample preparation and degassing procedures employed at Florida State University (FSU) have been described.^{21,22} Sets of 13 mm o.d. Pyrex tubes fitted with standard taper joints and grease traps were loaded with 3 mL aliquots of each concentration of DPB and *trans*-stilbene. They were degassed using at least six freeze–pump–thaw cycles to about 10^{−5} Torr and flame-sealed at a constriction. All operations, including analyses, were performed under nearly complete darkness (red light). UV absorption measurements in the course of the irradiation were carried out either by providing the Pyrex irradiation ampules with side arms consisting of a graded seal and a quartz UV cell or by periodically opening ampules and recording the UV spectra in standard UV cells. Irradiations were carried out in a Moses merry-go-round²³ apparatus immersed in a thermostatted water bath. A heating coil connected to a thermoregulator (Polyscience Corp.) was used to control the temperature to ±0.5 °C. The photoisomerization of *trans*-stilbene was used for actinometry, $\phi_{t \rightarrow c} = 0.52$.²¹ Hanovia 450 W medium-pressure Hg lamps (Ace Glass, Inc.) were employed. The 313 nm Hg line was isolated using a potassium perchromate/potassium carbonate filter solution in parallel with Corning CS 7-54 filter plates, as previously described.²¹

Photoisomerization in methylcyclohexane (MCH) was carried out at SCU as previously described,²⁰ except that this time, excitation was with a 337 nm pulsed nitrogen laser (Avco-Everett). Potassium ferrioxalate was used for actinometry. Stirred Ar-outgassed samples were irradiated in a 1 cm quartz stoppered fluorescence cell inside of a brass cell holder. Temperature was controlled with a Neslab Endocal refrigerated circulating bath system using propylene glycol.

Analytical Procedures. Analysis of stilbene isomerization was by GC, as described previously.²⁴ Analysis of DPB isomerization was either by GC, by HPLC, or by principal component analysis (PCA) of UV spectral matrices. A Varian 3300 gas chromatograph equipped with an electronic integrator was used with a DB-5 capillary column (17 m). Analyses were carried out at 12 psi of He and an initial temperature of 170 °C held for 10 min followed by 1 °C/min ramp to 190 °C. Detector and injector temperatures were set at 250 °C. Pentane was replaced by CCl₄ prior to GC analysis, and cyclohexane and benzene were replaced by hexane prior to HPLC analysis. Solvent removal was achieved by evaporation under a stream of Ar, and care was taken to avoid dryness. The HPLC analyses were done at ambient temperature on a normal-phase SI column (Beckman, ultrasphere, analytical,

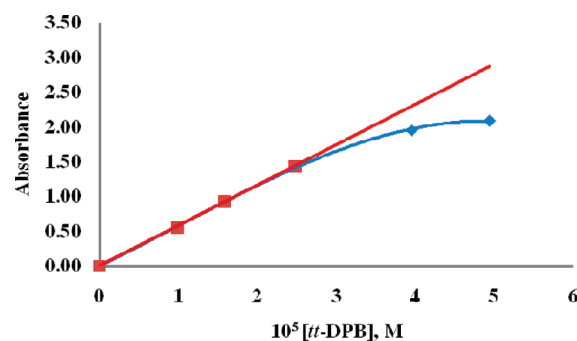


Figure 1. Beer–Lambert plot in PFH (garnet line through first four points).

4.6 × 250 mm) using optima hexanes (Fisher, optima) as the mobile phase (absorbance monitored at 315 nm). Electronic absorption spectra were recorded at 20 °C on a Varian Cary 300B UV–vis spectrophotometer using a thermostatted cell holder.

Absorption spectra in MCH were measured as a function of irradiation time with a Shimadzu UV-3101PC spectrophotometer. DPB isomer concentrations were determined by analysis of the absorption spectra. Quantum yields for photoisomerization of *tt* → *ct*-DPB were determined by use of Zimmerman's method.²⁵

Fluorescence Measurements. Fluorescence spectra were measured with a Hitachi F-4500 spectrophotometer equipped with a 150 W Xe arc source and a Hamamatsu R3788 photomultiplier tube. Fluorescence spectra were recorded for degassed, air-saturated, and Ar-bubbled solutions of *tt*-DPB in benzene in standard 1 cm² quartz cells. There was no oxygen effect on fluorescence intensity. Temperature was maintained at 20.0 ± 0.1 °C using a Neslab-RTE 4DD constant-temperature circulation bath and was monitored continuously during each scan with an Omega Engineering Model 199 RTD digital thermometer in a reference cell placed in the same constant-temperature cell holder. Absorption spectra were recorded with a Cary 300 UV–vis spectrophotometer at 20.0 °C. Absorbances at the excitation wavelengths were less than 0.1. Quinine sulfate in 1 N H₂SO₄ ($\phi_f = 0.546$, at 25 °C)^{26,27} was used as a reference standard. The solvent index of refraction correction was applied.

RESULTS

Solvent Effect on *tt*-DPB Absorptivity. *tt*-DPB solutions in hexane (H), cyclohexane (CH), benzene (Bz), and perfluorohexane (PFH) were made by dilution of CH stock solutions ($[tt\text{-DPB}] = 7.21 \times 10^{-3}$ M for CH, H, and Bz and 9.87×10^{-3} M for PFH) using λ -pipettes and volumetric flasks. In CH, H, and Bz, the five identical *tt*-DPB concentrations employed in the range of $0.721\text{--}3.60 \times 10^{-5}$ M gave excellent Beer–Lambert plots (CH contamination was in the 0.10–0.5% range in Bz and H and 0.25–4% in PFH). The plot in PFH has a downward curvature due to saturation but is linear for the three lowest concentrations, Figure 1. The Beer–Lambert plots in the other three solvents were strictly linear throughout the concentration range. Molar absorptivity coefficients, ϵ , at λ_{max} are given in Table 1.

Fluorescence Quantum Yield. The fluorescence quantum yield of *tt*-DPB in Bz was determined by exciting degassed, Ar-outgassed, and air-saturated solutions at 315, 330, and 345 nm. There was no oxygen-quenching effect within the

Table 1. Solvent Effect on Molar Absorptivities of *tt*-DPB^a

| solvent | λ_{\max} , nm | $10^{-4}\epsilon_{\max}$, M ⁻¹ cm ⁻¹ | $10^{-4}\epsilon_{313}^{tt}$, M ⁻¹ cm ⁻¹ | $10^{-4}\epsilon_{313}^{ct}$, M ⁻¹ cm ⁻¹ |
|---------|-----------------------|---|---|---|
| PFH | 318.5 | 5.82 | 4.82 | 2.98 |
| H | 328.0 | 5.51 (5.60) ^b | 4.62 | 3.05 |
| CH | 330.4 | 5.50 (5.42) ^c | 4.44 | 3.00 |
| Bz | 334.5 | 5.10 | 3.22 | 2.76 |

^a The last two columns show molar absorptivity values at 313 nm for *tt*- and *ct*-DPB, respectively. ^b From ref 18. ^c From ref 20.

Table 2. *tt*-DPB Photoisomerization in Degassed Hexane, 313 nm, ~22 °C^a

| <i>t</i> , min | f_{ct}^t | f_{cc}^t | f_{ct}^{corr} | f_{cc}^{corr} |
|---|------------|-------------|------------------------|------------------------|
| [<i>tt</i> -DPB] = 5.02 × 10 ⁻⁴ M | | | | |
| 0 | 0.0072(7) | 0 | 0 | 0 |
| 20 | 0.143(2) | 0.00291(2) | 0.153 | 0.00311 |
| 40 | 0.249(2) | 0.00532(9) | 0.301 | 0.00606 |
| 60 | 0.320(4) | 0.00692(30) | 0.421 | 0.00825 |
| 120 | 0.489(4) | 0.0106(5) | 0.834 | 0.01434 |
| 900 | 0.697(1) | 0.0221(4) | | |
| 1200 | 0.698(5) | 0.0232(2) | | |
| [<i>tt</i> -DPB] = 3.01 × 10 ⁻³ M | | | | |
| 0 | 0.018 | 0 | 0 | 0 |
| 20 | 0.0391(14) | 0.00048(2) | 0.022 | 0.000485 |
| 40 | 0.068(2) | 0.00132(26) | 0.0533 | 0.00136 |
| 60 | 0.0875(4) | 0.00157(15) | 0.0753 | 0.00163 |
| 120 | 0.148(18) | 0.00313(7) | 0.148 | 0.00337 |
| 900 | 0.501(1) | 0.0128(3) | | |
| 1200 | 0.56(3) | 0.0159(5) | | |

^a Values in parentheses are deviations from the mean for multiple GC injections; parallel irradiation of the *trans*-stilbene actinometer for 40 and 1200 min gave 38.5(3) and 93.3(3)% *cis*-stilbene, respectively.

experimental uncertainty of the measurements, and none was expected in view of the reported very short (29 ps)¹² *tt*-DPB fluorescence lifetime. The average of the nine values gave $\phi_f = 0.251 \pm 0.015$.

Photochemical Observations. *Hexane.* Concentrations of *tt*-DPB in hexane (3.01×10^{-3} and 5.02×10^{-4} M) were selected to roughly correspond to the highest and lowest concentrations employed in earlier work.²⁸ An intermediate concentration (1.69×10^{-3} M) of *trans*-stilbene in pentane was used for actinometry ($\phi_{t \rightarrow c} = 0.52$).²¹ Ampoules, immersed in water at room temperature (~22 °C), were irradiated in parallel in the merry-go-round. Conversions were measured by GC as a function of time, Table 2. They were corrected for zero-time isomer content and back reaction^{21,29} using eq 1

$$f_{cx}^{\text{corr}} = f_{cx}^{\text{eq}} \ln \left(\frac{f_{cx}^{\text{eq}} - f_{cx}^0}{f_{cx}^{\text{eq}} - f_{cx}^t} \right) \quad (1)$$

with the poststationary state (PSS) isomer composition fractions determined for the lower [DPB]: 0.279, 0.698, and 0.0226 for f_{tt}^{eq} , f_{ct}^{eq} and f_{cc}^{eq} , respectively. The other symbols in eq 1, f_{cx}^0 , f_{cx}^t and f_{cx}^{corr} , where *x* is *t* or *c*, are the zero-time fraction, the observed fraction at time *t*, and the corrected fraction, respectively.

Plots of the results in Table 2 are shown in Figure 2. Curves are drawn through observed conversions, and straight lines are

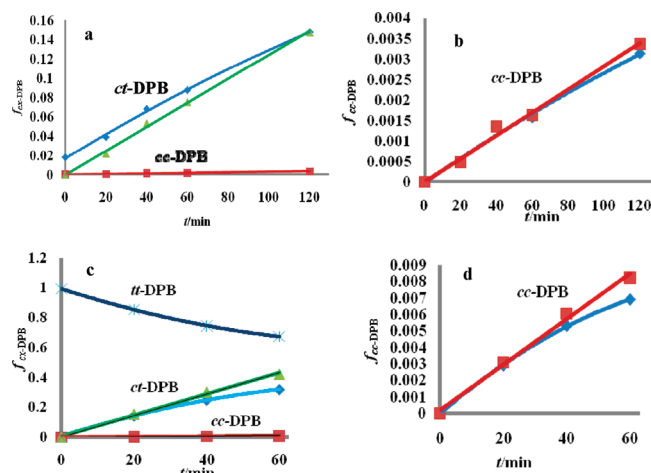


Figure 2. Photoisomerization of *tt*-DPB in H (upper and lower panels are for [*tt*-DPB] = 3.01×10^{-3} and 5.02×10^{-4} M, respectively); b and d panels are expanded plots of conversions to *cc*-DPB.

drawn through conversions that are corrected for zero-time contamination and back reaction. Direct formation of *cc*-DPB is demonstrated in panels b and d of Figure 2 by the absence of an induction period; the *cc*-DPB versus time plots are linear from the onset.

Cyclohexane, Methylcyclohexane, and Benzene Temperature Effect. Degassed aliquots (3 mL) of *tt*-DPB solutions in CH and Bz were irradiated in triplicate at 10 °C intervals in the thermostatted water bath in which the merry-go-round was immersed. Quantum yields were based on conversions for the first two tubes, which were irradiated for 50 and 120 min, respectively. The third tubes of each set were irradiated for 29–58 h to yield the PSS isomer compositions used for back reaction corrections. Ampoules containing *trans*-stilbene in pentane were irradiated in parallel for actinometry. Isomer compositions were determined by HPLC for DPB and by GC for stilbene (see above). The solvents, cyclohexane and benzene, were carefully replaced with hexane, and the solutions were concentrated to a maximum volume of 1 mL under a stream of Ar. HPLC measurements were performed with the UV detector set at 315 nm. Hexane was used as the eluent. HPLC areas were converted to relative molar contributions with the use of the molar absorptivities in ref 18. All operations were carried out under red light. The lower absorbance of *cc*-DPB (a factor of 2 lower than that for *tt*-DPB¹⁸ at 315 nm) coupled with its inefficient formation made it impractical to determine conversions of that isomer for quantum yield purposes. The actinometer $\phi_{t \rightarrow c} = 0.52$ at 30 °C²¹ was adjusted for the *T* change on the basis of the *T* dependence of ϕ_f of *trans*-stilbene (the change was 0.50₉–0.52₄ in the 10–40 °C range).³⁰ Identical changes were predicted using the Arrhenius parameters in ref 21 or the Eyring

Table 3. Photoisomerization Quantum Yields of *tt*-DPB in CH and Bz^a

| <i>T</i> , °C | $\phi_{tt \rightarrow ct}$ | | PSS ^b : $f_{tt}^{eq}, f_{ct}^{eq}, f_{cc}^{eq}$ | |
|---------------|--------------------------------------|-----------------------|--|----------------------------------|
| | CH | Bz | CH | Bz |
| 10.0 | 0.097 ₅ (2 ₅) | | 0.270, 0.711, 0.019 ₂ | |
| 20.0 | 0.11 ₅ (1) | 0.21 ₆ (1) | 0.319, 0.661, 0.019 ₅ | 0.341, 0.646, 0.012 ₇ |
| 30.0 | 0.12 ₆ (0) | 0.26 ₀ (2) | 0.276, 0.699, 0.024 ₉ | 0.306, 0.673, 0.020 ₈ |
| 40.0 | 0.13 ₆ (0) | 0.30 ₀ (5) | 0.239, 0.732, 0.029 ₇ | 0.294, 0.684, 0.022 ₁ |

^aThe concentrations employed were in the $(1.05\text{--}1.27) \times 10^{-3}$ and $(1.8\text{--}2.8) \times 10^{-4}$ M ranges for *t*-St and *tt*-DPB, respectively; values in parentheses are deviations from the mean in the last significant figures shown for duplicate determinations. ^bIrradiation times for PSS determinations (given in $f_{tt}^{eq}, f_{ct}^{eq}, f_{cc}^{eq}$ sequence) were 58, 40, 40, and 29 h for the 10, 20, 30, and 40 °C samples, respectively.

Table 4. Photoisomerization Quantum Yields of *tt*-DPB in MCH^a

| <i>T</i> , °C | $\phi_{tt \rightarrow ct}$ | $10^8 k_d^b, s^{-1}$ | <i>T</i> , °C | $\phi_{tt \rightarrow ct}$ | $10^8 k_d^b, s^{-1}$ |
|---------------|-------------------------------------|----------------------|---------------|-------------------------------------|----------------------|
| −5.3 | 0.054 (7) | 11.66 | 40.0 | 0.14 ₆ (1 ₉) | 23.77 |
| 7.2 | 0.07 ₂ (1 ₁) | 13.39 | 50.0 | 0.17 ₈ (2 ₁) | 29.15 |
| 20.0 | 0.12 ₀ (1 ₅) | 16.33 | | | |

^aValues in parentheses are deviations from the mean in the last significant figures shown for duplicate determinations. ^bInterpolated fluorescence decay rate constants from the Supporting Information in ref 16 (see text).

parameters in ref 30. Averages of duplicate quantum yields are shown in Table 3.

Quantum yields determined at SCU in MCH with the use of Zimmerman's method²⁵ are shown in Table 4. Light intensity was determined with the use of potassium ferrioxalate actinometry.³¹ Because a considerably longer excitation wavelength (337 nm) was employed than in the earlier work (325 nm),²⁰ the $\phi_{tt \rightarrow ct}$ value was also determined in CH at room temperature with 337 nm excitation and was found to be 0.11, that is, identical to the previously published value.²⁰

Perfluorohexane. The low solubility of *tt*-DPB in PFH precluded use of GC or HPLC analyses for the determination of isomer distributions in that solvent. Ampoules containing solutions of the DPB isomers were provided with 1 cm square quartz cell side arms for measurement of UV spectra in the course of the irradiation. Samples of *tt*-DPB in PFH were irradiated in the merry-go-round at room temperature (~ 23 °C) in parallel with *tt*-DPB samples in CH and in Bz. In addition, *trans*-stilbene actinometry was employed. Sets of UV spectra obtained in the course of 313 nm irradiation of each DPB isomer are shown in the panels b–d of Figure 3. They were recorded at 25.0 °C in a thermostatted cell holder. Pure DPB isomer spectra in PFH are shown in Figure 3a. Analogous pure component spectra and spectral evolutions starting from *tt*- and *cc*-DPB were observed in the other solvents, in agreement with previously reported results.^{18,20,32}

Spectral sets in each solvent were subjected to principal component analysis (PCA), as previously described.³³ Three principal component matrices were obtained in each solvent. Component fractional contributions, f_{xx}^n , for the normalized (to unit

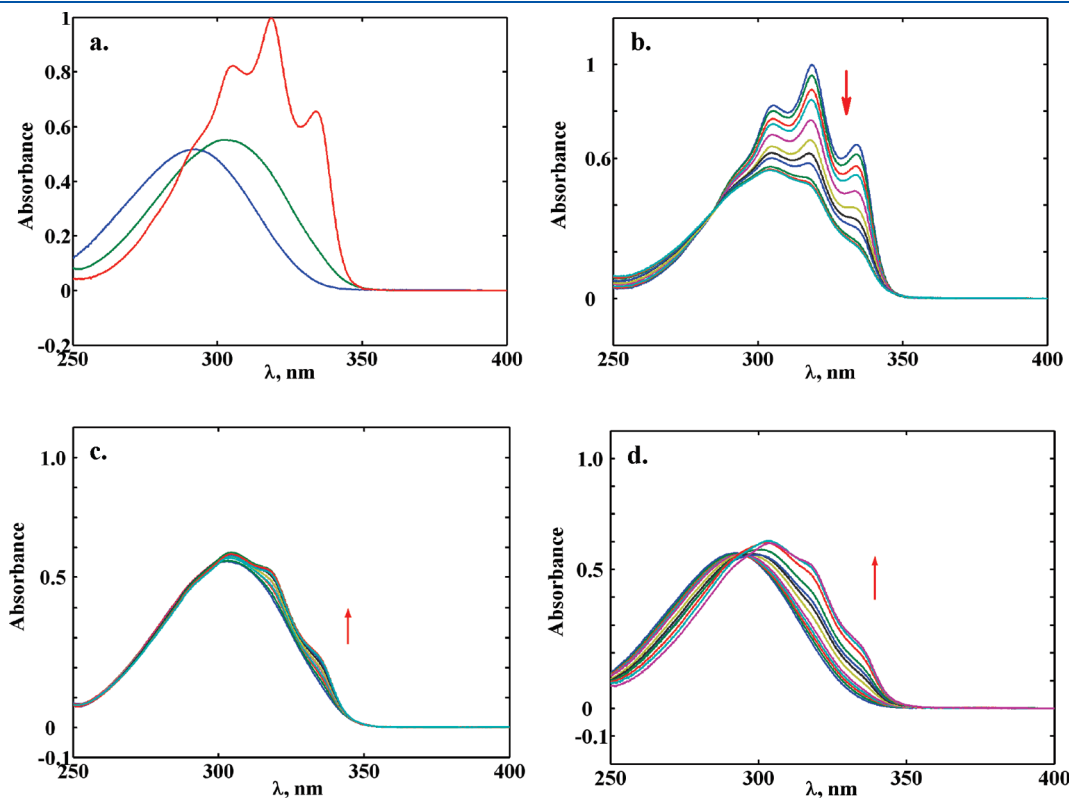


Figure 3. Photoisomerization of the DPBs in PFH; (a) Pure isomer spectra *tt*-, *ct*-, and *cc*-DPB in red, green, and blue, respectively; (b–d) starting from *tt*-, *ct*-, and *cc*-DPB, respectively.

area) spectra used in PCA were converted to molar fractional contributions, f_{ex}^t , by dividing each by the expected molar area (prior to normalization) of the corresponding pure component spectrum, A_i , at the initial [DPB] and adjusting to unity the sum of the resulting values, eq 2.

$$f_{\text{ex}}^t = \frac{f_{\text{ex}}^n/A_{\text{ex}}}{\sum_i f_i^n/A_i} \quad (2)$$

Viewed in eigenvector space, the plot of the combination coefficients, Figure 4, for the normalized spectra in Figure 2 is instructive. All spectra fall on the normalization plane defined by the three principal eigenvectors. The three pure component spectra define the corners of the normalization triangle containing eigenvector combination coefficients for spectra of all real mixtures of the three isomers. Starting from *tt*- and *cc*-DPB, initial mixture spectra fall on the *tt*-/*ct*-DPB and *cc*-/*ct*-DPB edges of the triangle, consistent with one-photon/one-bond photoisomerization, as initially reported by Zechmeister and co-workers.¹⁸ The PCA treatment of the UV spectra is not sufficiently accurate to reveal the small two-bond *tt* → *cc*-DPB photoisomerization channel that was observed by GC analysis in H.

Figure 5 shows relative photoisomerization rates in CH, PFH, and Bz, starting from *tt*- and *cc*-DPB. PCA derived conversions starting from *tt*-DPB were corrected for back reaction, eq 1. No back reaction corrections were applied to *cc*-DPB photoisomerization conversions because the low contribution of that isomer in the PSS ensures that its formation is virtually irreversible. However, because the PCA treatments of the spectral sets

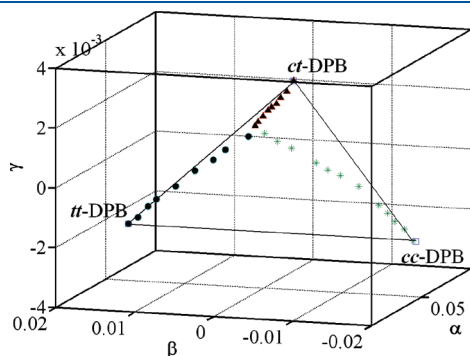


Figure 4. Combination coefficient plot from the PCA treatment of the spectra in Figure 3.

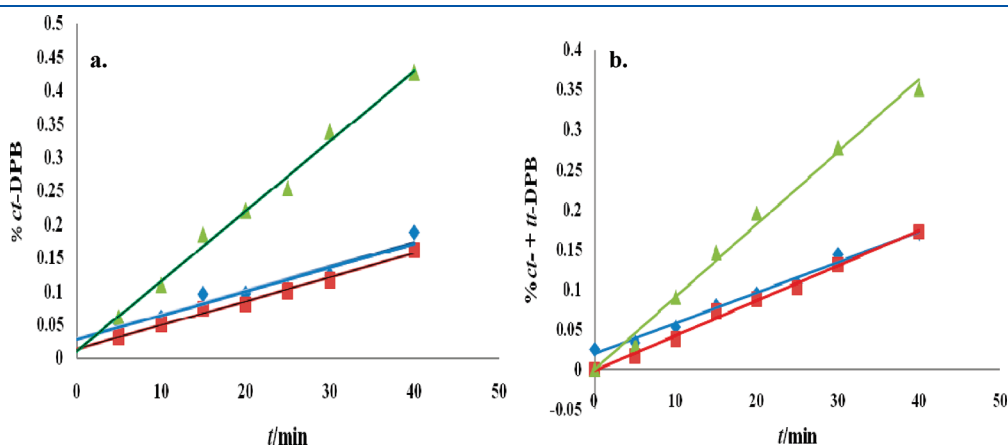


Figure 5. Relative *tt*- and *cc*-DPB photoisomerization conversions in CH (garnet ■), PFH (blue ◆), and Bz (green ▲), panels a and b, respectively.

revealed that excitation of photoproduct *ct*-DPB converts it mainly to *tt*-DPB, the yields of the two products were combined to obtain the true measure of *ct*-DPB formation, Figure 5b.

Table 5 gives the slopes s of the lines in Figure 5, which are the relative photoisomerization rates. They were converted to photoisomerization quantum yields using *t*-St actinometry, Table 5. Comparison with the more accurate quantum yields in Table 3 shows the $\phi_{\text{tt} \rightarrow \text{ct}}$ values to be in reasonable agreement, with small deviations in opposite directions in CH and in Bz. The estimated uncertainty in the PFH values is $\pm 15\%$.

DISCUSSION

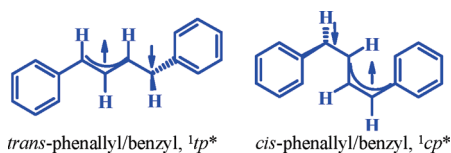
The *cis*–*trans* photoisomerization of the DPBs was first studied by Zechmeister and co-workers in H.¹⁸ They showed that upon irradiation in hexane, both *tt*- and *cc*-DPB are converted to the same *ct*-DPB-rich photostationary state.^{18b} Photoisomerization quantum yields, $\phi_{\text{tt} \rightarrow \text{ct}} = 0.25$ and $\phi_{\text{ct} \rightarrow \text{tt}} = 0.19$, were first reported in Bz by Whitten and co-workers.³² They reported that excitation of *tt*-DPB at either 313 or 366 nm in Bz leads to quasi-stationary states that, in addition to *tt*-DPB, include 60 and 64% *ct*-DPB, respectively, and 1–2% *cc*-DPB. They adopted the mechanism involving one bond twist (OBT) to phenallyl/benzyl intermediates that had been proposed for the photoisomerization of excited singlet³⁴ and triplet states³⁵ of alkyl-substituted 1,3-butadienes, Chart 1.³² A more complete study of DPB photoisomerization in CH was reported by Yee and co-workers.²⁰ Surprisingly, $\phi_{\text{tt} \rightarrow \text{ct}} = 0.11$, obtained upon 325 nm excitation, was even lower than the value in Bz. Quantum yields starting from the other isomers were similarly low, $\phi_{\text{cc} \rightarrow \text{ct}} = 0.20$ and $\phi_{\text{ct} \rightarrow \text{tt}} = 0.04$. Accordingly, the conclusion in both studies was that, in Bz and CH, significant radiationless decay channels of the

Table 5. PCA-Derived Isomerization Rates of *tt*- and *cc*-DPB in CH, PFH, and Bz, 313 nm, 23 °C^a

| solvent | 10 ⁵ [DPB] ₀ , M | | s , %/min | | $f_{\text{ct}}^{\text{eq}}$ | $\phi_{\text{tt} \rightarrow \text{ct}}$ | $\phi_{\text{cc} \rightarrow \text{ct}}$ |
|---------|--|----------------|----------------|----------------|-----------------------------|--|--|
| | <i>tt</i> -DPB | <i>cc</i> -DPB | <i>tt</i> -DPB | <i>cc</i> -DPB | | | |
| CH | 3.60 | 6.19 | 0.003549 | 0.004353 | 0.71 | 0.08 ₇ | 0.19 |
| PFH | 3.11 | 6.31 | 0.003552 | 0.003814 | 0.721 | 0.07 ₆ | 0.17 |
| Bz | 3.49 | 6.60 | 0.010585 | 0.009077 | 0.64 | 0.26 ₅ | 0.42 |

^a Parallel irradiation (30 min) of [*t*-St] = 2.38×10^{-3} M gave 9.12% (9.58%, corrected) *c*-St.

Chart 1



singlet excited states of the DPB isomers compete with torsional relaxation leading to isomerization. Related observations by Görner led to the same conclusion.³⁶ In agreement with Whitten and co-workers, Yee et al. proposed that *tt*- and *cc*-DPB photoisomerize via the intermediates in Chart 1 by the OBT processes $^1tt^* \rightarrow ^1tp^*$ and $^1cc^* \rightarrow ^1cp^*$. Both intermediates are accessible from $^1ct^*$. Because *cc*-DPB was not detected by HPLC analysis at 300 nm, the *cis*-phenallyl/benzyl intermediate was assumed to decay exclusively to *ct*-DPB. More recently, Krishna and Singh reported a sharp increase in *tt*-DPB photoisomerization quantum yields (330 nm, hexane, 25 °C) as the concentration of *tt*-DPB was increased (a factor of 4.67 in $\phi_{tt \rightarrow ct}$ over the 0.62–3.08 $\times 10^{-3}$ M range).²⁸

Quantum Yields. The combination coefficient plot for PFH in Figure 4 is a representative example. We obtained similar plots in CH and Bz. Starting from the *tt*- and *cc*-DPB tetrahedron corners, spectral points initially move on the *tt*-/*ct*- and *cc*-/*ct*-DPB edges, respectively, consistent with one-photon/one-bond photoisomerization, as had been previously concluded.^{18,20,32} However, as the GC results in H show, due to the very small *cc*-DPB contribution to photostationary states, the adherence of initial points to two-component edges can be deceiving. Accordingly, UV analysis fails to reveal the presence of significant decay channels to *cc*-DPB.

The photoisomerization quantum yields determined in our work at ambient *T* are summarized in Table 6 together with literature values of fluorescence lifetimes and quantum yields (except that ϕ_f in Bz is from this work). Our $\phi_{tt \rightarrow ct}$ values in Bz and CH agree exactly with the literature values. In contrast to the report by Krishna and Singh,²⁸ we find that $\phi_{tt \rightarrow ct}$ in H is not concentration-dependent. Our 0.092 value is somewhat larger than 0.084, the value reported for the highest concentration employed in that work.²⁸ If the proposed interpretation of fluorescence data¹⁶ were correct, one would expect that $\phi_{tt \rightarrow ct}$ would be largest in PFH. On the contrary, that is the solvent in which the $\phi_{tt \rightarrow ct}$ value is smallest. Our photoisomerization quantum yields starting from *cc*-DPB exhibit the same trend, being largest in Bz and smallest in PFH. Despite the considerable range in quantum yields, PSS compositions are relatively solvent-independent (see the Hexane subsection and Tables 3 and 5). The contribution of *ct*-DPB is largest in all cases, and the contribution of *cc*-DPB never exceeds 3%. Consistent with past practice,^{20,32} we neglected the small contribution of *cc*-DPB and used the molar absorptivities at 313 nm and the equilibrium isomer fractions determined in this work to calculate the $\phi_{ct \rightarrow tt}$ values in Table 6

$$\phi_{ct \rightarrow tt} = \phi_{tt \rightarrow ct} \left(\frac{\epsilon_{tt}^{313} f_{tt}^{eq}}{\epsilon_{ct}^{313} f_{ct}^{eq}} \right) \quad (3)$$

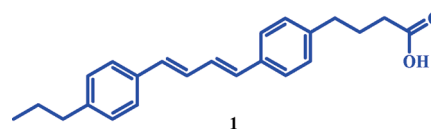
Bicycle Pedal Channel. Noteworthy is our observation that ~20% of the photoisomerization of *tt*-DPB in H goes directly to *cc*-DPB. GC analysis would probably have revealed small

Table 6. Solvent Effect on *tt*-DPB Photoisomerization and Fluorescence Quantum Yields, ~20 °C^a

| solvent | τ_f /ns | ϕ_f | $10^8 k_f$ s ⁻¹ | $\phi_{tt \rightarrow ct}$ | $\phi_{tt \rightarrow cc}$ | $\phi_{ct \rightarrow tt}$ | $\phi_{cc \rightarrow ct}$ | ϕ_{ic} |
|---------|--------------|----------|----------------------------|---------------------------------------|----------------------------|----------------------------|----------------------------|-------------|
| Bz | 0.30 | 0.25(2) | 8.3 | 0.25, 0.25 ^b | | 0.16, 0.19 ^b | 0.42 | 0.25 |
| MCH | 0.59 | 0.36 | 6.1 | 0.12 | | | | 0.40 |
| CH | 0.57 | 0.41 | 7.2 | 0.11 _s , 0.11 ^c | | 0.066, 0.04 ^f | 0.19 | 0.36 |
| H | 0.48 | 0.36 | 7.5 | 0.092, 0.084 ^d | 0.020 | 0.060 | | 0.48 |
| PFH | 0.20 | 0.038 | 1.9 | 0.07 ₆ | | 0.15 | 0.17 | 0.81 |

^a In H and CH, τ_f and ϕ_f values are averages of those compiled in Table 2 of ref 16; PFH values are from ref 16; the τ_f in Bz is the average from refs 12 and 37, and the ϕ_f is from this work. ^b From ref 32. ^c From ref 20. ^d From ref 28.

Chart 2



contributions of direct formation of *cc*-DPB in the other solvents. Simultaneous two-bond photoisomerization is consistent with Warshel's bicycle pedal (BP) mechanism.³⁸ This volume-conserving process was proposed for space-confining media such as the protein environments of the retinyl moieties in rhodopsin and bacteriorhodopsin that could inhibit the large torsional displacements to orthogonal geometries that are associated with the usual OBT mechanism. BP predicts the net chemical process in the light-adaptation photocycles of bacteriorhodopsin (13-*cis*-15-*syn* \rightarrow 13-*trans*-15-*anti*)³⁹ and *Anabaena* sensory rhodopsin (13-*trans*-15-*anti* \rightarrow 13-*cis*-15-*syn*).^{40,41} The BP mechanism reduces free volume requirements by confining most of the motion to the vicinity of the isomerizing double bonds while minimizing the motion of bulky substituents. Indeed, we recently observed two-bond DPB photoisomerization in the opposite direction (*cc*-DPB \rightarrow *tt*-DPB) in glassy media at low T ⁴² and in the solid state.⁴³ There are other solid-state examples of photoisomerization consistent with the BP mechanism.⁴⁴ Less common are reports of BP products in solution. The interconversion of *ctt*- and *tct*-DPH could involve simultaneous two-bond photoisomerization.^{17a,b} Another possible example is the adiabatic photoisomerization of *cis,cis*-1,4-di(3,5-di-*tert*-butylstyryl)-benzene to *trans,trans*-1,4-di(3,5-di-*tert*-butylstyryl)benzene.⁴⁵ Related studies in the distyrylbenzene family have revealed similar results.⁴⁶ Most intriguing is Whitten's proposal of BP photoisomerization for the *tt*-DPB moiety covalently embedded in the alkyl chain of the carboxylic acid **1**, Chart 2.⁴⁷ The change in mechanism from OBT to BP was proposed to account for the much lower *T* sensitivity of the radiationless decay of **1** relative to the unsubstituted parent *tt*-DPB.

Medium constraints are absent in solution, and sequential, instead of concerted, isomerization of the two bonds in **1** cannot be ruled out. The two-bond interconversion of *trans*, *trans*- and *cis,cis*-2,4-hexadiene triplets was shown to proceed via rapid equilibration of *trans*-allylmethylene and *cis*-allylmethylene triplet intermediates,^{35c} and an analogous process could account for the formation of *cc*-DPB from *tt*-DPB. Possible *tt*-DPB photoisomerization pathways are shown in Chart 3.

Solvent Effect on the $1^1B_u/2^1A_g$ State Order. Before considering the significance of the solvent effect on the DPB

Chart 3

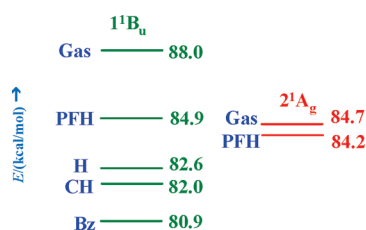
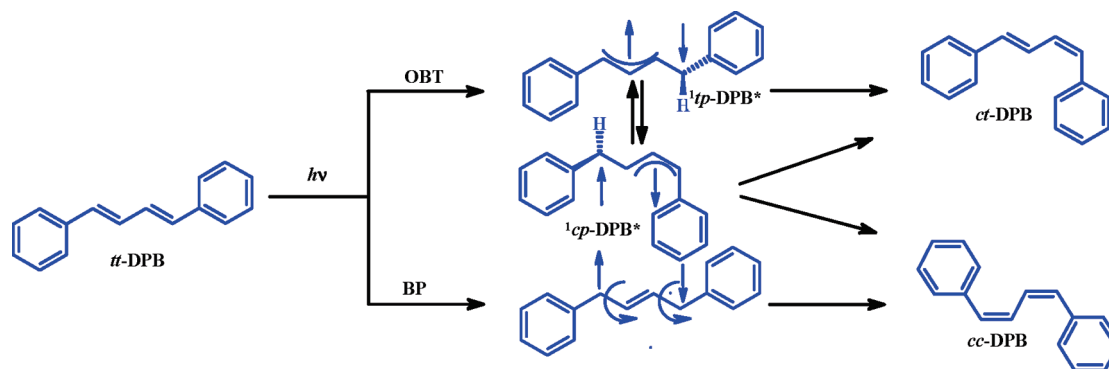


Figure 6. Medium effect on the lowest two singlet excited states of *tt*-DPB.

photoisomerization quantum yields, we must briefly review the extensive literature on the influence of the solvent on the relative energy of the two lowest singlet excited states of *tt*-DPB.⁴⁸ Absorption and fluorescence of *tt*-DPB involve the symmetry-allowed $1^1A_g \rightarrow 1^1B_u$ transition in all solvents studied thus far.^{12–16,49,50} However, one-photon^{51,52} and two-photon^{52,53} fluorescence excitation spectra of *tt*-DPB in the gas phase, seeded in He in a jet expansion, firmly establish that the 2^1A_g state lies 3.3 kcal/mol below the 1^1B_u state under isolated molecule conditions. In the free jet expansion where *tt*-DPB molecules have low vibrational and rotational temperatures and there are no collisions, mode-selective fluorescence lifetimes, ranging up to 100 ns,^{51–53} are consistent with a forbidden electronic transition, and the fluorescence quantum yield is unity at 0 excess energy.⁵⁴ The sharp decrease in the fluorescence quantum yield and lifetime with increasing excitation energy has been attributed to the onset of a nonradiative channel associated with isomerization at about 1100 cm^{-1} above the 2^1A_g zero-point energy level. Excitation of a static *tt*-DPB gas at $95\text{ }^\circ\text{C}$ gives the $2^1A_g \rightarrow 1^1A_g$ emission spectrum, but upon thermal equilibration in the presence of added PFH vapor, that spectrum is replaced by the allowed $1^1B_u \rightarrow 1^1A_g$ emission spectrum.^{49,50}

The $1^1B_u \leftarrow 1^1A_g$ transition energy decreases with increasing medium polarizability, being linearly dependent on $\alpha = (n^2 - 1)/(n^2 + 2)$, where n is the refractive index.^{49,55,56} On the other hand, the forbidden $2^1A_g \leftarrow 1^1A_g$ transition energy is almost polarizability-independent. Consequently, as shown in Figure 6, the low polarizability of PFH leads to reversal of the $2^1A_g/1^1B_u$ energy order so that, whereas S_1 is the 1^1B_u state in all hydrocarbon solvents, S_1 is the 2^1A_g state in PFH.^{49,50} We can now readily understand the sharp drop in the k_f value of *tt*-DPB in PFH, Table 6. Most excited singlet states occupy the nonfluorescent 2^1A_g state in PFH, and

fluorescence arises from the small equilibrium population of molecules in the 1^1B_u state. Accordingly, k_f^{eff} , the effective radiative rate constant, is given by

$$k_f^{\text{eff}} = k_f^B e^{-\Delta E/RT} \quad (4)$$

where k_f^B is the radiative rate constant of the 1^1B_u state and ΔE is the $2^1A_g/1^1B_u$ energy gap. The theoretical value of $k_f^B = 6.7 \times 10^8\text{ s}^{-1}$ in CH, based on the Birks–Dyson modification⁵⁷ of the Strickler–Berg relationship,⁵⁸ is in reasonable agreement with the experimental values in Table 6 for the hydrocarbon media. Taking into account the smaller PFH index of refraction and the larger *tt*-DPB molar absorptivities in PFH (Table 1), the k_f value for H of $7.5 \times 10^8\text{ s}^{-1}$ in Table 6 was adjusted to $6.8 \times 10^8\text{ s}^{-1}$ for PFH. Substitution of that k_f^B value and $\Delta E = 0.7\text{ kcal/mol}$ from Figure 6 into eq 4 gives $k_f^{\text{eff}} = 2.0 \times 10^7\text{ s}^{-1}$, in excellent agreement with the value for PFH in Table 6.

We note that our interpretation of the radiative rate constant of *tt*-DPB in PFH differs sharply from that given by Maroncelli and co-workers.¹⁶ They assumed that the *tt*-DPB radiative rate constant is a continuous function of solvent polarizability and fitted values in hydrocarbon and fluorocarbon solvents in a single plot that includes the experimental value of $1.54 \times 10^7\text{ s}^{-1}$ that had been assigned to the $2^1A_g \rightarrow 1^1A_g$ transition of the isolated molecule in the gas phase.⁵⁴ Their model assumes the lowest excited singlet state to be a single, strongly mixed ($2^1A_g + 1^1B_u$) state rather than an equilibrium mixture of two distinct states, one mainly A_g -like and the other mainly B_u -like, as assumed here.

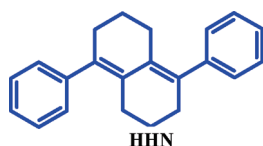
Competing Radiationless Decay Channels. The internal conversion quantum yields listed in the last column of Table 6, were obtained from the experimental fluorescence and photoisomerization quantum yields using

$$\phi_{ic} = 1 - \phi_f - 2\phi_{tt \rightarrow ct} - \phi_{tt \rightarrow cc} \quad (5)$$

In eq 5, it is assumed that the *trans*-phenallyl/benzyl intermediate, 1^1tp-DPB^* , in Chart 3 decays with equal probability to *tt*-DPB and *ct*-DPB, as suggested by Yee and co-workers.^{1,20} The small difference in the $\phi_{ic} = 0.36$ value for CH in Table 6 and the reported 0.34 value is due to use of $\phi_f = 0.42$ and inclusion of a small intersystem crossing contribution, $\phi_{is} = 0.02$, in the earlier work.²⁰ Because experimental values for ϕ_f of *tt*-DPB in CH are in the 0.39–0.44 range,¹⁶ we used the average value of 0.41.

The ϕ_{ic} 's in Table 6 range from a low value of 0.25 in Bz to a high value of 0.81 in PFH; the opposite trend applies to the

Chart 4



photoisomerization quantum yields. Photoisomerization is most efficient in the highly polarizable Bz in which the 1^1B_u state is the lowest excited singlet state, Figure 6, and the ΔE_{ab} gap is largest, and it is least efficient in PFH in which the 2^1A_g state is the lowest excited singlet state. We conclude that photoisomerization does not involve crossing from the 1^1B_u into the 2^1A_g state as proposed in the Birks extension of the OS mechanism to α,ω -diphenylpolyenes.^{10,11} The most reasonable alternative explanation is that the 1^1B_u state is the reactive state, as had been proposed by Troe and co-workers.^{14a}

The deactivation of 1tt -DPB* by an internal conversion step not leading to photoisomerization was first proposed to account for smaller than expected photoisomerization quantum yields in Bz by Whitten and co-workers³² and in CH by Yee and co-workers.²⁰ A $k_{ic} = 2.5 \times 10^8 \text{ s}^{-1}$ value in H was calculated by Velsko and Fleming on the basis of the nonlinear T dependence of total nonradiative decay constants¹² in H, and similar values were estimated in the n -alkanes by Troe and co-workers.^{14a} Because those estimated k_{ic} values are too small to account for the low photoisomerization quantum yields, Troe and co-workers suggested that the assumption in eq 5 of equal partitioning from the twisted singlet excited intermediate to the ground states of tt - and ct -DPB isomers does not hold for DPB. They proposed a decay ratio for 1tp -DPB* (Chart 3) of 3–4 in favor of tt -DPB and assumed that torsional relaxation to the twisted intermediate (presumably, 1tt -DPB* \rightarrow 1tp -DPB*) is the dominant nonradiative decay path of the planar excited state. We can offer three objections to this interpretation. First, decay from twisted triplet and singlet excited stilbene intermediates, although usually assumed to give the two ground-state isomers with equal probability, actually favors *cis*-stilbene, the higher-energy isomer.^{3b,21} If the analogy holds, decay from 1tp -DPB* should favor the higher-energy ct -DPB isomer. Second, the corollary to the proposed preferential decay of 1tp -DPB* to tt -DPB is that, assuming the same intermediate, ct -DPB \rightarrow tt -DPB photoisomerization quantum yields should be unusually large. The low $\phi_{ct \rightarrow tt}$ values in Table 6 show that, in all solvents studied thus far, this expectation is not borne out. Third, fluorescence lifetimes of 1,5-diphenyl-2,3,4,6,7,8-hexahydronaphthalene (HHN, Chart 4), indicate that internal conversion rate constants exhibit similar Arrhenius behavior as those of tt -DPB and are larger than those of tt -DPB, despite the fact that in HHN, photoisomerization is structurally inhibited.⁵⁹ Alkyl substitution in this structural analogue of tt -DPB is expected to increase the energy gap between the 2^1A_g and 1^1B_u states,²² and it is reasonable to conclude that facile radiationless decay pathways are available to the 1^1B_u state of HHN that do not require large torsional displacement in the diene unit. It is difficult to understand, however, why such pathways are not similarly effective in **1**.

As can be seen in Table 6, 81% of 1tt -DPB* molecules in PFH undergo internal conversion without photoisomerization. The dominant contribution of an unreactive 1tt -DPB* radiationless decay pathway to the overall decay rate in PFH brings into question the significance of theoretical treatments¹⁶ that are

based on the assignment of all radiationless decay to torsional relaxation. Whether the competing internal conversion pathway involves decay of the 2^1A_g state directly to the 1^1A_g state or via the 1^1B_u state remains to be established and should be a challenge for theory to predict.

Temperature Effects on Nonradiative Decay. The T dependence of torsional decay rate constants can be derived from the photoisomerization quantum yields in CH (Table 3) and MCH (Table 4) and the known T dependence of the fluorescence lifetimes^{12,16} using

$$\alpha k_{\text{tors}} = \phi_{tt \rightarrow ct} / \tau_f \quad (6)$$

Table 4 includes fluorescence decay rate constants, interpolated from the experimental values in ref 16 using a trinomial fit of the decay constant dependence on T . Arrhenius plots of the product of torsional rate constants and the decay fraction α of the assumed 1tp -DPB* intermediate, αk_{tors} , and of the total radiationless decay rate constants, k_{nr} , from refs 12 and 16, are shown in Figure 7. In both CH and MCH, those plots are almost parallel but have significantly different intercepts. In CH, the activation energies, E_a , are 5.3 and 4.9 kcal/mol, and pre-exponential factors, A , are 8.0×10^{12} and $1.7 \times 10^{12} \text{ s}^{-1}$ (assuming $\alpha = 0.5$, independent of T) for k_{nr} and k_{tors} , respectively. The corresponding values in MCH are $E_a = 5.4$ and 6.6 kcal/mol, and the pre-exponential factors are $A = 1.04 \times 10^{13}$ and $3.10 \times 10^{13} \text{ s}^{-1}$ in the same order. In each solvent, the E_a values for k_{nr} and k_{tors} are the same within experimental uncertainty, especially if one considers that we have confined our treatment of the decay rate constants in MCH in ref 16 to those provided in the Supporting Information for that paper. The more extensive data set plotted in Figure 7 of that paper gives $E_a = 6.4$ kcal/mol and $A = 5.45 \times 10^{13} \text{ s}^{-1}$, but the three additional k_{nr} values at lower T than that in Figure 7b, where the fluorescence lifetime is dominated by radiative decay, are subject to larger experimental uncertainty. The finding of experimentally indistinguishable activation energies for overall radiationless decay as for photoisomerization is consistent with Troe's proposal that decay from the *trans*-phenallyl/benzyl intermediate gives mainly tt -DPB. If 1tt -DPB* \rightarrow 1tp -DPB* were the only radiationless decay process, we could infer from the ratio of the pre-exponential values that α would have to be as small as 0.10 and 0.28 in CH and MCH, respectively. However, as pointed out above, this is not likely in view of the small $\phi_{ct \rightarrow tt}$ values in Table 6. We refrain from attaching undue significance to the A values because narrow T ranges are involved, and small errors in the slopes of the Arrhenius plots in Figure 7 lead to large errors in the intercepts.

If reactive radiationless decay from 1tt -DPB* leads to ct -DPB via 1tp -DPB*, it follows that unreactive radiationless decay does not reach that intermediate. Assuming that the identity of the activation energies is not a coincidence, one can imagine that, in hydrocarbon solvents, unreactive and reactive radiationless decays of 1tt -DPB* are on the same trajectory, but torsional displacement in the shared transition state stops short of that required for reaching a 90° twisted intermediate. Photoisomerization might then occur via inefficient leakage from that transition state to 1tp -DPB*. Alternatively, 1tp -DPB* may not be on the reaction pathway, and photoisomerization may occur inefficiently, following internal conversion, by continuation in the ground state of the small excited-transition-state torsional displacement. Momentum considerations for continuation of motion from the excited to the ground state may apply in the

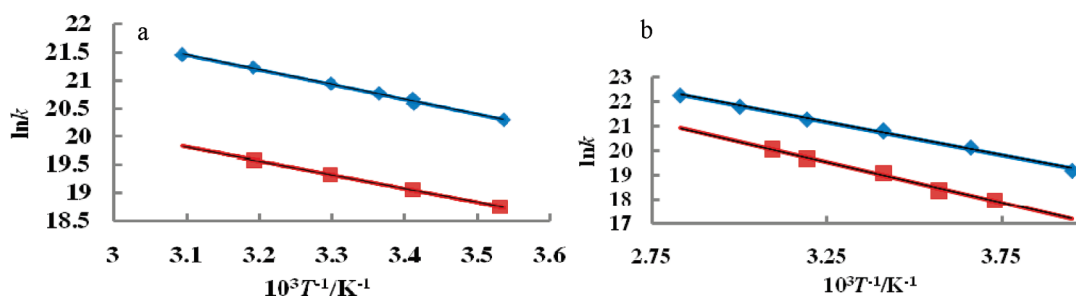


Figure 7. Arrhenius plots of αk_{tors} (red ■) and k_{nr} (blue ◆) in CH, panel a, and MCH, panel b.

latter case.⁶⁰ Decay via a conical intersection that is attained by a relatively small torsional distortion would be consistent with observations on HHN, the structurally constrained *tt*-DPB analogue, Chart 4. We stress here that proper interpretation of the effect of medium friction on ¹*tt*-DPB* radiationless decay must be based on knowledge of the molecular motion with which the medium interferes. We have shown that the usual assumption that that motion is torsional displacement leading to ¹*tp*-DPB* is not correct.

Our results on the *T* dependence of ¹*tt*-DPB* radiationless decay are in contrast to observations on *tt*-DPH, for which photoisomerization was shown to be subject to much higher activation energies than those obtained from the overall radiationless decay rate constants.^{17c}

The possible *T* dependence of the relative contribution of OBT and BP photoisomerization channels remains to be established. Simultaneous two-bond photoisomerization accounts for 20% of the photoisomerization events in H at ~23 °C, and its contribution may change with *T* and with medium viscosity.

Preliminary attempts to measure the *T* dependence of photoisomerization quantum yields in PFH have been stymied primarily due to solubility problems. However, the shorter fluorescence lifetime and smaller photoisomerization quantum yield in that solvent at 20 °C lead us to expect large discrepancies between activation parameters for the photoisomerization path and for overall radiationless decay. The low photoisomerization quantum yield in this solvent shows that ready access to the ²¹A_g state suppresses the photoisomerization channel instead of enhancing it, as would be expected if the Birks extension of the OS mechanism applied. Consistent with this conclusion is the observation that photoisomerization is most efficient in Bz, the solvent in which the ²¹A_g state is least accessible. We conclude that the ²¹A_g state is not involved as a photoisomerization intermediate. Fast ²¹A_g → ¹¹A_g internal conversion could account for the short *tt*-DPB fluorescence lifetime in PFH.

CONCLUSIONS

Our observations on the photoisomerization of the 1,4-diphenylbutadiene isomers in solution complement previous work on the stilbenes^{2,3,7,21,61} and the 1,6-diphenylhexatrienes.^{17,22} The first three members of the α,ω -diphenylpolyene family exhibit strikingly different photophysical and photochemical behavior. Controlling factors are the proximity and energetic order of the ¹¹B_u and ²¹A_g states, their two lowest electronically excited singlet states. Photoisomerization in the singlet-state manifold is most efficient in *t*-St, for which S₁ is the ¹¹B_u state, and least efficient in *ttt*-DPH, for which S₁ is the ²¹A_g state, although in *ttt*-DPH, reversing the ²¹A_g/¹¹B_u state order does not enhance photoisomerization.²² In *tt*-DPB,

photoisomerization is most efficient in Bz, where S₁ is the ¹¹B_u state and the ΔE_{ab} energy gap is largest, and least efficient in PFH, where S₁ is the ²¹A_g state. Because efficient population of the ²¹A_g state hampers photoisomerization instead of facilitating it, the Birks extension¹¹ of the OS model¹⁰ for photoisomerization to α,ω -diphenylpolyenes is not valid and must be abandoned.

The OS model for stilbene photoisomerization¹⁰ is, itself, of questionable validity. The increased polarizability accompanying the change from the gas phase to a hydrocarbon medium stabilizes the ¹¹B_u state of *t*-St by about 5 kcal/mol.⁵⁶ Because, by analogy with *tt*-DPB and *ttt*-DPH, the ²¹A_g state should be insensitive to the polarizability change, the OS model predicts a substantial increase in the torsional barrier of *t*-St upon moving from the isolated molecule in the gas phase to solution. The actual change, from 3.3 ± 0.2 kcal/mol^{2,62,63} in the gas phase to an intrinsic barrier of 2.9 kcal/mol in *n*-alkanes,^{30,61b} is, if anything, in the opposite direction. The possibility that the torsional barrier is created by the crossing of the ¹¹B_u state with a higher A_g excited state⁶⁴ is no more attractive because that barrier should also increase with increasing medium polarizability. It appears, therefore, that the torsional barrier is a property of the ¹¹B_u state, a position that was championed by Troe and Weitzel.⁶⁵

The large contributions of ¹*tt*-DPB* radiationless decay pathways that do not lead to photoisomerization, in all solvents studied, and especially in PFH, bring into question explanations of medium effects on ¹*tt*-DPB* fluorescence lifetimes that assign all radiationless decay to the photoisomerization channel.

AUTHOR INFORMATION

Corresponding Author

*E-mail: saltiel@chem.fsu.edu.

ACKNOWLEDGMENT

This research was supported by the National Science Foundation, most recently by Grant No. CHE-0846636.

REFERENCES

- (1) Allen, M. T.; Whitten, D. G. *Chem. Rev.* **1989**, *89*, 1691–1702.
- (2) Saltiel, J.; Sun, Y.-P. In *Photochromism, Molecules and Systems*; Dürr, H. Bouas-Laurent, H., Eds.; Elsevier: Amsterdam, The Netherlands, 1990; pp 64–164.
- (3) (a) Saltiel, J. *J. Am. Chem. Soc.* **1967**, *89*, 1036–1037. (b) Saltiel, J. *J. Am. Chem. Soc.* **1968**, *90*, 6394–6400.
- (4) Malkin, S.; Fischer, E. *J. Phys. Chem.* **1964**, *68*, 1153.
- (5) Sharafi, S.; Muszkat, K. A. *J. Am. Chem. Soc.* **1971**, *93*, 4119.
- (6) Sumitani, A.; Nakashima, N.; Yoshihara, K.; Nagakura, S. *Chem. Phys. Lett.* **1977**, *51*, 183.

- (7) (a) Charlton, J. L.; Saltiel, J. *J. Phys. Chem.* **1977**, *81*, 1940–1944. (b) Saltiel, J.; Charlton, J. L. *Cis-Trans Isomerization of Olefins. In Rearrangements in Ground and Excited States*; de Mayo, P., Ed.; Academic Press: New York, 1980; Vol III, pp 25–89.
- (8) Hudson, B. S.; Kohler, B. E. *Annu. Rev. Phys. Chem.* **1974**, *25*, 437–460.
- (9) Hudson, B. S.; Kohler, B. E.; Schulten, K. In *Excited States*; Lim, E. C., Ed.; Academic Press: New York, 1982; Vol. 6, pp 1–95.
- (10) Orlandi, G.; Siebrand, W. *Chem. Phys. Lett.* **1975**, *30*, 352–354.
- (11) (a) Birks, J. B.; Birch, D. J. S. *Chem. Phys. Lett.* **1975**, *31*, 608–610. (b) Birks, J. B.; Tripathy, G. N. R.; Lumb, M. D. *Chem. Phys.* **1978**, *33*, 185–194. (c) Birks, J. B. *Chem. Phys. Lett.* **1978**, *54*, 430–434.
- (12) Velso, S. P.; Fleming, G. R. *J. Chem. Phys.* **1982**, *76*, 3553–3562.
- (13) Birch, D. J. S.; Imhof, R. E. *Chem. Phys. Lett.* **1982**, *88*, 243–247.
- (14) (a) Gehrke, C.; Mohrschladt, R.; Schroeder, J.; Troe, J.; Vöhringer, P. *Chem. Phys.* **1991**, *152*, 45–56. (b) Mohrschladt, R.; Schroeder, J.; Schwarzer, D.; Troe, J.; Vöhringer, P. *J. Chem. Phys.* **1994**, *101*, 7566–7579. (c) Schroeder, J.; Steinel, T.; Troe, J. *J. Phys. Chem. A* **2002**, *106*, 5510–5516 and references cited.
- (15) (a) Anderton, R. M.; Kauffmann, J. E. *J. Phys. Chem.* **1994**, *98*, 12117–12124. (b) Anderton, R. M.; Kauffmann, J. E. *J. Phys. Chem.* **1994**, *98*, 12125–12132. (c) Anderton, R. M.; Kauffmann, J. E. *J. Phys. Chem.* **1995**, *99*, 14628–14631.
- (16) Dahl, K.; Biswas, R.; Maroncelli, M. *J. Phys. Chem. B* **2003**, *107*, 7838–7853.
- (17) (a) Saltiel, J.; Ko, D.-H.; Fleming, S. A. *J. Am. Chem. Soc.* **1994**, *116*, 4099–4100. (b) Saltiel, J.; Wang, S.; Watkins, L. P.; Ko, D.-H. *J. Phys. Chem. A* **2000**, *104*, 11443–11450. (c) Saltiel, J.; Krishnamoorthy, G.; Huang, Z.; Ko, D.-H.; Wang, S. *J. Phys. Chem. A* **2003**, *107*, 3178–3186.
- (18) (a) Sandoval, A.; Zechmeister, L. *J. Am. Chem. Soc.* **1947**, *69*, 553–557. (b) Pickard, J. H.; Wille, B.; Zechmeister, L. *J. Am. Chem. Soc.* **1948**, *70*, 1938–1944.
- (19) Saltiel, J.; Dmitrenko, O.; Pillai, Z. S.; Klima, R.; Wang, S.; Wharton, T.; Huang, Z.-N.; van de Burgt, L. J.; Arranz, J. *Photochem. Photobiol. Sci.* **2008**, *7*, 566–577.
- (20) Yee, W. A.; Hug, S. J.; Kliger, D. S. *J. Am. Chem. Soc.* **1988**, *110*, 2164–2169.
- (21) Saltiel, J.; Marinari, A.; Chang, D. W.-L.; Mitchener, J. C.; Megarity, E. D. *J. Am. Chem. Soc.* **1979**, *101*, 2982–2996.
- (22) Saltiel, J.; Wang, S. *Photochem. Photobiol. Sci.* **2006**, *5*, 883–895.
- (23) Moses, F. G.; Liu, R. S. H.; Monroe, B. M. *Mol. Photochem.* **1969**, *1*, 245–249.
- (24) Saltiel, J.; Ganapathy, S.; Werking, C. *J. Phys. Chem.* **1987**, *91*, 2755–2758.
- (25) Zimmerman, G.; Chow, L.-Y.; Paik, U.-J. *J. Am. Chem. Soc.* **1958**, *80*, 3528–3531.
- (26) Melhuish, W. H. *J. Phys. Chem.* **1961**, *65*, 229–235.
- (27) Meech, S. R.; Phillips, D. *J. Photochem.* **1983**, *23*, 193–217.
- (28) Krishna, T. S. R.; Singh, A. K. *Indian J. Chem.* **1994**, *33B*, 413–414.
- (29) Lamola, A. A.; G. S. Hammond, G. S. *J. Chem. Phys.* **1965**, *43*, 2129–2135.
- (30) (a) Saltiel, J.; Sun, Y.-P. *J. Phys. Chem.* **1989**, *93*, 6246–6250. (b) Sun, Y.-P.; Saltiel, J. *J. Phys. Chem.* **1989**, *93*, 8310–8316.
- (31) Murov, S. L. *Handbook of Photochemistry*; Marcel-Dekker: New York, 1973.
- (32) Eastman, L. R., Jr.; Zarnegar, B. M.; Butler, J. M.; Whitten, D. G. *J. Am. Chem. Soc.* **1974**, *96*, 2281–2282.
- (33) (a) Saltiel, J.; Cires, E.; Turek, A. *J. Am. Chem. Soc.* **2003**, *125*, 2866–2867. (b) Sun, Y.-P.; Sears, D. F., Jr.; Saltiel, J. *Anal. Chem.* **1987**, *59*, 2515–2519.
- (34) Saltiel, J.; Metts, L.; Wrighton, M. *J. Am. Chem. Soc.* **1970**, *92*, 3227–3229.
- (35) (a) Saltiel, J.; Metts, L.; Wrighton, M. *J. Am. Chem. Soc.* **1969**, *91*, 5684–5685. (b) Saltiel, J.; Metts, L.; Sykes, A.; Wrighton, M. *J. Am. Chem. Soc.* **1971**, *93*, 5302–5303. (c) Saltiel, J.; Rousseau, A. D.; Sykes, A. *J. Am. Chem. Soc.* **1972**, *94*, 5903–5905. (d) Saltiel, J.; Townsend, D. E.; Sykes, A. *J. Am. Chem. Soc.* **1973**, *95*, 5968–5973.
- (36) Görner, H. *J. Photochem.* **1982**, *19*, 343–356.
- (37) Keery, K. M.; Fleming, G. R. *Chem. Phys. Lett.* **1982**, *93*, 322–326.
- (38) Warshel, A. *Nature (London)* **1976**, *260*, 679–683.
- (39) Harbison, G. S.; Smith, S. O.; Pardo, J. A.; Winkel, C.; Lugtenburg, J.; Herzfeld, J.; Mathies, R.; Griffin, R. G. *Proc. Natl. Acad. Sci. U.S.A.* **1984**, *81*, 1706–1709.
- (40) Sineshchekov, O. A.; Trivedi, V. D.; Sasaki, J.; Spudich, J. L. *J. Biol. Chem.* **2005**, *280*, 14663–14668.
- (41) Wada, Y.; Kawanabe, A.; Furutani, Y.; Kandori, H.; Ohtani, H. *Chem. Phys. Lett.* **2008**, *453*, 105–108.
- (42) (a) Saltiel, J.; Krishna, T. S. R.; Turek, A. M.; Clark, R. J. *J. Chem. Soc.: Chem. Commun.* **2006**, 1506–1508. (b) Saltiel, J.; Bremer, M. A.; Laohhasurayotin, S.; Krishna, T. S. R. *Angew. Chem., Int. Ed.* **2008**, *47*, 1237–1240.
- (43) (a) Saltiel, J.; Krishna, T. S. R.; Clark, R. J. *J. Phys. Chem. A* **2006**, *110*, 1694–1697. (b) Saltiel, J.; Krishna, T. S. R.; Laohhasurayotin, S.; Fort, K.; Clark, R. J. *J. Phys. Chem. A* **2008**, *112*, 199–209.
- (44) (a) Odani, T.; Matsumoto, A.; Sada, K.; Miyata, M. *Chem. Commun.* **2001**, 2004–2005 and references therein. (b) Matsumoto, A. *Top. Curr. Chem.* **2005**, *254*, 263–305. (c) Nishizawa, N.; Furukawa, D.; Kobatake, S.; Matsumoto, A. *Cryst. Growth Des.* **2010**, *10*, 3203–3210. (d) Sonoda, Y.; Kawanishi, Y.; Tsuzuki, S.; Goto, M. *J. Org. Chem.* **2005**, *70*, 9755–9763.
- (45) Sandros, K.; Sundhal, M.; Wennerström, O.; Norinder, U. *J. Am. Chem. Soc.* **1990**, *112*, 3082.
- (46) (a) Aiorba, S.; Galiazzo, G.; Mazzucato, U.; Spalletti, A. *J. Phys. Chem. A* **2010**, *114*, 10761–10768. (b) Bartocci, G.; Ciorba, S.; Mazzucato, U.; Spalletti, A. *J. Phys. Chem. A* **2009**, *113*, 8557–8568 and previous papers in this series..
- (47) Allen, M. T.; Miola, L.; Whitten, D. G. *J. Phys. Chem.* **1987**, *91*, 6099–6102.
- (48) For a comprehensive critical review of spectroscopic literature through 1989 see ref 2.
- (49) Itoh, T.; Kohler, B. E. *J. Phys. Chem.* **1988**, *92*, 1807–1813.
- (50) Itoh, T. *Chem. Phys. Lett.* **2001**, *342*, 550–554.
- (51) Heimbrook, L. A.; Kohler, B. E.; Spiglianin, T. A. *Proc. Natl. Acad. Sci. U.S.A.* **1983**, *80*, 4580–4584.
- (52) Shepanski, J. F.; Keelan, B. W.; Zewail, A. H. *Chem. Phys. Lett.* **1983**, *103*, 9–14.
- (53) Horwitz, J. S.; Kohler, B. E.; Spiglianin, T. A. *J. Chem. Phys.* **1985**, *83*, 2186–2190.
- (54) Amirav, A.; Sonnenschein, M.; Jortner, J. *Chem. Phys.* **1986**, *102*, 305–312.
- (55) Hudson, B. S.; Kohler, B. E. *J. Chem. Phys.* **1973**, *59*, 4984–5002.
- (56) Sklar, L. A.; Hudson, B. S.; Petersen, M.; Diamond, J. *Biochemistry* **1977**, *16*, 813–818.
- (57) Birks, J. B.; Dyson, D. J. *Proc. R. Soc. London, Ser. A* **1963**, *275*, 135–148.
- (58) Strickler, S. J.; Berg, R. A. *J. Chem. Phys.* **1963**, *37*, 814–822.
- (59) Yee, W. A.; Horwitz, J. S.; Goldbeck, R. A.; Einterz, C. M.; Kliger, D. S. *J. Phys. Chem.* **1983**, *87*, 380–382.
- (60) Weiss, R. M.; Warshel, A. *J. Am. Chem. Soc.* **1979**, *101*, 6131–6133.
- (61) (a) Saltiel, J.; Waller, A. S.; Sears, D. F., Jr. *J. Am. Chem. Soc.* **1993**, *115*, 2453–2465. (b) Saltiel, J.; Waller, A. S.; Sears, D. F., Jr.; Garrett, C. Z. *J. Phys. Chem.* **1993**, *97*, 2516–2522.
- (62) (a) Syage, J. A.; Lambert, W. R.; Felker, P. M.; Zewail, A. H.; Hochstrasser, R. M. *Chem. Phys. Lett.* **1982**, *88*, 266–270. (b) Syage, J. A.; Felker, P. M.; Zewail, A. H. *J. Chem. Phys.* **1984**, *81*, 4706–4723. (c) Felker, P. M.; Zewail, A. H. *J. Chem. Phys.* **1985**, *89*, 5402–5411.
- (63) Majors, T. J.; Even, U.; Jortner, J. *J. Chem. Phys.* **1984**, *81*, 2330–2338.
- (64) Hohlneicher, G.; Dick, B. *J. Photochem.* **1984**, *27*, 215–231.
- (65) Troe, J.; Weitzel, K. M. *J. Chem. Phys.* **1988**, *68*, 7030–7039.